Published in final edited form as:
Biochemistry. 2012 March 27; 51(12): 2630–2637. doi:10.1021/bi300157r.

Schiff Base Protonation Changes in Siberian Hamster Ultraviolet Cone Pigment Photointermediates †

Victoria L. Mooney[‡], **Istvan Szundi**[§], **James W. Lewis**[§], **Elsa C. Y. Yan**[‡,*], and **David S. Kliger**[§,*]

Department of Chemistry, Yale University, New Haven, CT 06520

Department of Chemistry and Biochemistry, University of California, Santa Cruz, CA 95064

Abstract

Molecular structure and function studies of vertebrate ultraviolet (UV) cone visual pigments are needed to understand the molecular evolution of these photoreceptors, which uniquely contain unprotonated Schiff base linkages between the 11-*cis* retinal chromophore and the opsin proteins. In this study, the Siberian hamster ultraviolet cone pigment (SHUV) was expressed and purified in an n-dodecyl-β-D-maltoside suspension for optical characterization. Time-resolved absorbance measurements, over a spectral range from 300 to 700 nm, were made on the purified pigment at time delays from 30 ns to 4.64 seconds after photoexcitation using 7 ns pulses of 355 nm light. The resulting data were fit globally to a sum of exponential functions after noise reduction using singular value decomposition. Four exponentials best fit the data with lifetimes of 1.4 μs, 210 μs, 47 ms and 1 s. The first photointermediate species characterized here is an equilibrated mixture similar to the one formed after rhodopsin's Batho intermediate decays into equilibrium with its successor, BSI. The extremely large red shift of the SHUV Batho component relative to the pigment suggests that SHUV Batho has a protonated Schiff base and that the SHUV cone pigment itself has an unprotonated Schiff base. In contrast to SHUV Batho, the portion of the equilibrated mixture's spectrum corresponding to SHUV BSI is well fit by a model spectrum with an unprotonated Schiff base. The spectra of the next two photointermediate species revealed that they both have unprotonated Schiff bases and suggest they are analogous to rhodopsin's Lumi I and Lumi II species. After decay of SHUV Lumi II, correspondence with rhodopsin photointermediates breaks down and the next photointermediate, presumably including the G protein-activating species, is a mixture of protonated and unprotonated Schiff base photointermediate species.

Investigations of the molecular structure and function of vertebrate ultraviolet (UV) cone visual pigments are important to the understanding of molecular evolution of vertebrate visual pigments. Vertebrate visual pigments evolved such that contemporary pigments fall under five classifications: rhodopsin (RH1), rhodopsin-like (RH2), short wavelength-sensitive 1 and 2 (SWS1 and SWS2), and medium/long wavelength sensitive (M/LWS) (Figure 1) (1–4). Vertebrate UV cone pigments belong to the SWS1 class, which evolved from a common ancestor after the M/LWS class, which includes red and green cone pigments, but prior to rhodopsin.

†This research was supported by research grant EY00983 from the National Eye Institute of the National Institutes of Health to DSK and by a National Science Foundation Career Grant (MCB-0955407) to EY.

*Corresponding Author: David S. Kliger, phone (831) 459-2106, FAX (831) 459-2935, kliger@ucsc.edu. *Corresponding Author: Elsa C. Y. Yan, phone (203) 436-2509, FAX (203) 432-6144, elsa.yan@yale.edu.

As these pigment classes evolved, so did the absorption maxima of the pigments and the molecular structures controlling them. One characteristic that is known to significantly impact the absorption maxima of visual pigments is the protonation state of the Schiff base (SB) linkage through which the 11-cis retinal ligand attaches to a lysine residue in the opsin protein. Only those pigments with absorbance maxima in the UV possess Schiff bases which are unprotonated in the dark state; all others, including the rhodopsin rod pigments, possess protonated Schiff bases (PSBs). While some of the factors controlling the Schiff base protonation state, and thus the absorption maximum, of UV pigments have recently been identified (5), there is still much about these pigments and the characteristics that they acquired during pigment evolution that remains unknown (6).

Understanding how visual pigment absorbance maxima are controlled is important for vision, but it also has broader implications. Besides providing a more unified description of the pigments themselves, insight into the chemistry of the binding site is needed to understand the mechanism of photoactivation, since the same factors which control the absorbance wavelength of different pigments also control the absorbance changes of photointermediates in the activation process. Structural understanding of photointermediates, in turn, potentially gives insight into early activation steps of G protein-coupled receptors (GPCRs), a pharmaceutically important family whose other members are currently inaccessible to study by the time-resolved methods used here.

Prior to the development of suitable gene expression systems, purification difficulties impeded study of cone pigments' activation mechanisms. Furthermore, until gene expression systems became available, the quantities of cone pigments needed for time-resolved study could only be produced from species whose eyes were available as a by-product of food production. That excluded study of some interesting cone pigments, such as the UV cone pigment from the Siberian hamster (*Phodopus sungorus*), whose photointermediates we characterize here. The selective advantage conferred by UV pigments' significant extension of the visual range is only beginning to be understood. UV pigments appear to have been lost in close relatives of the Siberian hamster (7), and no basis for that loss in the UV pigment's properties has so far been found. UV absorbing pigments are also of fundamental chemical interest because, in spite of the fact that SB protonation functions both as a wavelength regulator and as a conformational lock, factors controlling SB protonation are still poorly understood. The work presented here is the first comprehensive time-resolved study of a UV cone pigment's activation mechanism allowing us to directly compare its pathway with that of rhodopsin, thus revealing how the photoactivation pathway of visual pigments evolved in parallel with its λ_{max}.

MATERIALS AND METHODS

Protein preparation

Preparation of the *Phodopus sungorus* (Siberian Hamster) UV pigment gene, its incorporation into a tetracycline inducible pACMV-TetO vector (8), and creation of a *GnTI*$^{-}$ HEK293S stable cell line was previously described (5). Protein preparation was also performed as previously described (5,8). Briefly, cells were grown on 10 cm tissue culture plates or in a BioFlo Celligen 310 fermentor/bioreactor and protein expression was induced upon addition of 5 mM sodium butyrate and 2μg/mL tetracycline. The cells were harvested 48 hr after induction. After addition of 11-*cis* retinal the protein was prepared under dim red light (5,6,9). The cells were solubilized in a solution containing 1% w/v n-dodecyl-β-D-maltoside and the protein purified via immunoaffinity chromatography, wherein the 1D5 epitope cloned into the C-terminus of the UV pigment was recognized by the 1D4 monoclonal antibody bound to agarose resin (9,10). The purified SHUV pigment was in a solution containing 47 mM HEPES, pH 6.6, 132 mM NaCl, 2.8 mM $MgCl_2$, 0.02% DM,

and 7.5% w/v glycerol. The resulting sample was concentrated to ~100 μL and the UV pigment quantified by UV-Vis spectroscopy using an extinction coefficient of 43,300 ± 700 $cm^{-1}M^{-1}$ at 359 nm (5).

Time-resolved absorbance measurements—Time-resolved absorbance changes from 300 to 700 nm were measured at 20 °C using an apparatus described previously (11). Instead of the dye laser excitation used there, samples were excited directly with the third harmonic of the Nd:YAG laser. Absorbance difference spectra ($A_{photolyzed}(\lambda) - A_{unphotolyzed}(\lambda)$) were collected at a series of delay times after the ~7 ns excitation pulse of 355 nm light (80 μJ/mm^2), beginning at 300 ns and ending at 4.64 seconds. Polarization of the linearly polarized probe light was set to 54.7 degrees (magic angle) relative to the excitation pulse polarization so that apparent absorbance changes due to rotational diffusion of SHUV would not be recorded. At some of the delay times, anomalies in the data were observed, apparently caused by thermal transients due to absorption of the 355 nm laser on the wall of the cell insert. Similar apparent absorbance transients were observed at the same time delays when the cell contained only water, and data presented here were corrected for these thermal effects by subtracting appropriate water baselines. A typical experiment used ~120 μg of pigment in 0.5 mL which produced an absorbance of ~0.04 in the 2 mm path length of the probe beam.

Data Analysis Using Global Fitting

Sets of time-dependent absorbance difference spectra (typically 40 averages at each delay time) were transformed using singular value decomposition, $\Delta A(\lambda,t) = \mathbf{USV}^{\dagger}$ (12), and noise was reduced by representing the data using only basis spectra in the **U** matrix which were associated with singular values above the level associated with noise. A nonlinear least squares method was used to determine the best fit of the data, $\Delta a(\lambda,t)$, in the following form:

$$\Delta a(\lambda, t) \equiv b_0(\lambda) + b_1(\lambda)e^{-t/\tau_1} + b_2(\lambda)e^{-t/\tau_2} + \ldots$$

with 3, 4 and 5 exponential terms (12). Global fitting gave the time constants, τ_i, for the exponential processes and the b-spectra, $b_i(\lambda)$ or spectral coefficients of terms decaying with those time constants, and $b_0(\lambda)$, which is the final difference spectrum extrapolated on our experimental time scale. The number of exponentials that best fit the data was determined from plots of residuals, $\Delta A(\lambda,t) - \Delta a(\lambda,t)$.

Even if the evolution of photointermediates follows the simplest mechanism, i.e. a unidirectional sequential model, A → B → C ..., the b-spectra do not correspond exactly to the difference spectra between successive photointermediates e.g. $b_2(\lambda)$ would not be equal to the difference $A_B(\lambda) - A_C(\lambda)$, because any sum of exponentials function results from a model which assumes all the time dependent spectral changes all start at t = 0. Clearly this assumption is not true for the simple sequential model above because formation of photointermediate C only begins at some delay after initial photolysis, specifically after photointermediate B is formed. The actual difference spectra between successive photointermediates for the above simplest, unidirectional sequential model must be constructed from linear combinations of the b-spectra (13). The difference spectra between successive photointermediates were constructed in that manner and are referred to here as unidirectional sequential intermediate difference (USID) spectra. After constructing the USID spectra, it is straightforward to convert them into absolute spectra of the unidirectional sequential intermediates (USIs) by adding back the spectrum of the pigment that was bleached to USID 1 to obtain USI 1 and constructing USI 2 by adding back USI 1 to USID 2 *etc*. However, individual USIs are not necessarily homogeneous photointermediates, but

instead one or more USIs could correspond to equilibrium mixtures. One way this occurs is when a significant back reaction rate exists in one of the sequential steps. In other cases, the time constant of equilibration may not be resolvable, as is the situation where a homogeneous photointermediate rapidly decays into equilibrium with another photointermediate on a time scale that is fast compared to its formation or compared to the decay of the mixture. In visual pigments, the equilibrium mixture character is typically manifested by USI spectra which are unusually broad or which have two maxima. Thus, the USI scheme is an artificial construct used as an initial approximation in the analysis so that the correct scheme, possibly including back reactions, can be finally determined.

RESULTS

Time-resolved absorbance data collected after photoexcitation of 1 μL Siberian hamster UV cone pigment aliquots is shown in Figure 2.

The time delays when data was collected were refined in a previous experiment (data not shown) which showed that only limited change occurred between 30 ns and 300 ns, but that significant change occurred between 240 ms and the time scale of seconds where benchtop spectrophotometers operate. By assuring that the final product observed in the time-resolved experiments was the same as that recorded in careful measurements with a conventional spectrophotometer, the spectrum of the bleached pigment could be better estimated for final reconstruction of absolute photointermediate spectra.

The data were best fit by a sum of four exponential terms with time constants (base e) of 1.4 μs, 210 μs, 47 ms and 1.0 second and a constant term, $b_0(\lambda)$. Figure 3 shows the b-spectra (coefficients) associated with those terms.

Although in general, the b-spectra are not identical to difference spectra between successive photointermediates or mixtures thereof, in the case of an unbranched mechanism with time constants that are well separated, as they are here, the difference between b-spectra and USID spectra is minor and within the noise level of the b-spectra determined here.

The first USID spectrum is the absorbance of the first photointermediate (or equilibrated mixture of photointermediates) minus the bleach i.e. the absorbance of the pigment that was photoisomerized by the 355 nm excitation pulse. USID 1 can be converted to the absolute spectrum of the first species formed, USI 1, by adding back the bleach and then the other absolute USI spectra can be sequentially computed from their precursors to yield the spectra shown in Figure 4.

While two of these, USI 2 and USI 3, have band shapes similar to the dark-state pigment itself and are thus likely to be homogeneous photointermediate species, USIs 1, 4 and 5 have either multiple bands or are broader, suggesting those photointermediates are equilibrated mixtures. The red-shifted character (relative to the original Siberian hamster UV pigment absorbance) of the 480 nm band in USI 1's spectrum and the time scale on which it appears are suggestive of the Batho intermediate which occurs after photoexcitation of bovine rhodopsin and other cone visual pigments (14–16) . However, the red shift is much larger than what would be expected from the usual chromophore torsion alone, so simple spectral modeling was used to explore possible assignments of the components of USI 1's absorbance.

Visual pigments' and their photointermediates' absorbance spectra generally show a trend for the width of the main absorbance band to become narrower, when viewed on a wavelength scale, as their maximum absorbance wavelength shifts to the blue (13,17). If instead of plotting on a wavelength scale, an energy scale is used for plotting absorbance, the width of

the model spectra representing rhodopsin photointermediates are much more constant (18). Narrowing in wavelength of a visual pigment absorbance band with blue shift of its maximum also occurs when the visible absorbing rhodopsin mutant E113Q is converted to the UV absorbing form in the absence of chloride ions (19). Similarly, Figure 5 shows the absorbance spectrum of the Siberian hamster UV cone pigment to be much narrower than the absorbance band of bovine rhodopsin. However, if the energy distribution corresponding to the breadth of the bovine rhodopsin's absorbance band is used to plot a band whose maximum is at 360 nm (18), as shown by the solid line in Figure 5, the agreement with the Siberian hamster UV cone pigment's absorbance band is excellent.

This observed consistency of energy band width, combined with the additional assumption that the energy shift induced by protonation of the chromophore Schiff base in the Siberian hamster UV cone pigment is constant, can be used to model the Siberian hamster UV cone photointermediate spectra as shown in Figure 6. The figure shows model spectra based on rhodopsin photointermediates with protonated and deprotonated chromophore Schiff bases compared with the photointermediate species observed after photoisomerization of Siberian hamster UV cone pigment.

There, the energetic shift of SB protonation uses the energy value corresponding to the shift from 360 nm to 440 nm observed after acidification of the pigment in the dark (5).

DISCUSSION

UV cone visual pigments absorb at significantly shorter wavelengths than the violet cone pigments absorb, with the histogram of cone pigment absorbance maxima in Figure 7 showing the peak of the UV group separated by ~60 nm from the violet group peak, and a wavelength gap of approximately 30 nm where no pigment's absorption maximum reproducibly occurs.

Presumably, these two groups differ in the protonation state of the N-retinylidene Schiff base, with the UV pigment's SB unprotonated and the violet pigment's SB protonated (20,21). However, this conjecture has so far only been verified directly by the study of mouse UV pigment and *xenopus laevis* violet cone pigment, where counterion mutants have been prepared showing the expected behavior (6). The time-resolved absorbance measurements reported here suggest that the Siberian hamster UV cone pigment also has an unprotonated SB in the dark and that near physiological temperatures, the first photointermediate, analogous to bathorhodopsin (Batho), has an unexpectedly large red shift due to photoisomerization induced protonation of the SB.

In the most extensively characterized visual pigment, bovine rhodopsin, the red shift of the first photointermediate, Batho, is approximately 30 nm, which has been attributed to torsional strain of the all-trans N-retinylidene chromophore (22–24). The idea that torsion, not charge separation between PSB and counterion, is responsible for the bulk of the Batho red shift in rhodopsin is supported by the observation that in the related unprotonated SB pigment, bovine rhodopsin's E113Q mutant at pH 8.2, the 24 nm red shift of Batho is very similar (particularly when converted from wavelength to energy). However, for the Siberian hamster UV cone pigment studied here, the expected energy shift due to torsion in the unprotonated SB form of the pigment (shown by the dotted line in the top, right panel of Figure 6) accounts for less than half the red shift in the absorbance observed for the long wavelength band of the first photointermediate. Instead, substantial additional red shift seems to be present and, as shown in Figure 6, can be accounted for by assuming the SB, unprotonated in the 11-cis pigment, protonates immediately after photoisomerization.

Siberian hamster UV Batho and BSI Differ in SB Protonation

In bovine rhodopsin at 20 °C, the decay of Batho into equilibrium with the second, blue-shifted intermediate (BSI) takes place with a lifetime of ~40 ns, which can be resolved in the type of experiments conducted here. However, this process could not be resolved after photoisomerization of the Siberian hamster UV cone pigment, as it apparently takes place more rapidly than it does in bovine rhodopsin. The situation is similar to what has been observed after photoexcitation of other cone pigments, such as chicken iodopsin and gecko P521, where the conversion of Batho into its equilibrium mixture with BSI is too fast to detect after excitation with ~10 ns laser pulses at 20 °C (15,16). The observation of accelerated Batho decay in a UV cone pigment suggests that the destabilization of Batho (compared to the bovine rhodopsin photointermediate) previously reported in two long-wave sensitive pigments (15,16) may be a more general cone pigment property.

An unusual feature of the equilibrated mixture which was detected here as the first photointermediate species, USI 1, is that while the Batho form has a protonated SB, the BSI component of the mixture has an unprotonated SB, similar to the original Siberian hamster UV cone pigment itself. Although crystal structure information is not available for any of the cone pigments, such data is available for bovine rhodopsin and for its first photointermediate, Batho, where the distance of the SB nitrogen from the oxygens of the counterion, Glu113 increases approximately 0.3 Å in Batho (25). Surprisingly, this was determined to be more due to a change in the position of Glu113 than as being due to a change in SB position. Movement of Glu113 would most likely arise from electrostatic changes i.e. delocalization of the PSB charge in the chromophore at Batho, which could shift the position of an adjacent charged group. Similar electrostatic changes associated with the torsionally strained SHUV Batho chromophore could be the direct cause of SB protonation upon Batho formation in Siberian hamster UV pigment by increasing electron density on its unprotonated SB.

Previously, we built molecular models of protonated photointermediates which might form early in the photoactivation pathway of the Siberian hamster UV pigment (5). One of these, considered to be a Batho equivalent, revealed that it is not only the Glu113 residue which determines the protonation state of the Schiff base. The water molecule that participates in the Glu113 network has the ability to switch the protonation state of the Schiff base in the UV pigment. In the dark state, Glu113 is in a Glu113··Ser90··H_2O··SB H-bond network. However, as the water molecule moves away from the unprotonated Schiff base, the Glu113 hydroxyl side chain reorients away from Ser90 and towards the Schiff base, allowing it to donate a proton. It is possible that this mechanism, wherein the position of this binding site water molecule determines the Schiff base protonation state, is employed throughout the rest of the photoactivation mechanism.

Due to the entropically favored nature of BSI in its equilibrium mixture with Batho, BSI does not accumulate at low temperatures (12), so even for bovine rhodopsin no crystal structure was possible for that photointermediate. However, rhodopsin's BSI has been attributed to a torsionally relaxed form (26) with weakened hydrogen bonding to the SB nitrogen (27). The former character, as a reversal of the property proposed here as stabilizing a protonated SB at Batho in the Siberian hamster pigment, and the latter character, as an additional electrostatic change at BSI, could both contribute to the reversion of BSI to a deprotonated SB. In any case, the spectrum of the UV band of USI 1, shown in the left upper panel of Figure 6 (points), clearly fits well to the band modeled from the energy shift of rhodopsin's BSI plus an additional energy shift attributable to deprotonation of the SB in the UV Siberian hamster cone pigment binding pocket. Without the deprotonation shift being added to the model SHUV BSI spectrum in PSB form (dotted line), the UV band data cannot be fit.

The only UV pigment whose photointermediates have been previously studied is the mouse UV sensitive cone pigment (MUV), and the methodology in those studies, low temperature trapping, was different from the time-resolved approach used here (28). There, a MUV Batho product was seen, and its stability temperature was consistent with Batho photointermediates from other visual pigments, but it retained an unprotonated SB over its thermal stability range. The observation of different MUV and SHUV Batho SB protonation states is surprising because the chromophore environment seems well conserved in the two proteins. An alternative explanation for the Batho SB protonation change is the approximately 100 K difference in temperature between the top of the temperature trapped MUV Batho stability range and our 20 °C measurements.

At low temperatures, MUV Batho was reported to decay through the Batho ⇄ BSI equilibrated mixture. Typically, the BSI photointermediate cannot be observed in temperature trapping experiments, so it was surprising that it was reported to be involved in MUV Batho decay (28). However, given the stabilizing temperatures reported there and in later work on a related pigment, it is likely that the BSI analog seen in MUV may bear more similarity to the Lumi I form seen in the D108A mutant of the *Xenopus laevis* violet cone pigment (VCOP), and it will be discussed as such below.

Two forms of SHUV Lumi

As has been seen in time-resolved absorbance measurements on bovine rhodopsin (29), the Batho ⇄ BSI equilibrated mixture decays through two Lumi intermediates which have absorbance bands whose width and maxima are similar to that of the SHUV pigment's dark state (Figure 4). In SHUV, the two Lumi photointermediates differ in absorbance strength by approximately 20%, allowing them to be resolved in our experiments. In the rhodopsin system, Lumi II has been determined to be the first photointermediate whose chromophore properties are affected by the protein environment (membrane or detergent). Thus by reciprocity, at the Lumi II stage, isomerization-induced change must have propagated well outside the chromophore pocket (29).

The increase in absorbance strength seen here during SHUV Lumi II formation is similar to an increase seen in the artificial UV pigment formed by the D108A mutation of VCOP when its Lumi II intermediate forms (28), although in VCOP-D108A protonation of the SB accompanies Lumi II formation. It is important to note that SB protonation states are secondary characteristics of photointermediates with their primary character being determined by their temperature/temporal stability range. Schiff base protonation may be more important as a probe of structure around the chromophore than as a driving force for structural change. A similar SB protonation has been reported to take place between the MUV Batho ⇄ BSI equilibrated mixture and its Lumi stage, which is our basis for considering the former to be more closely related to Lumi I, making the latter correspond to Lumi II (30). Overall, the similarity between the sequence of photointermediates up to Lumi II in all these visual pigments suggests that all have a similar fundamental mechanism which is unchanged even though differences in SB protonation exist in specific cases. In fact, the variation suggests that chromophore SB protonation has its primary role as a regulator of dark absorbance and that after photoisomerization it adopts a more passive, reporter character.

Late Photointermediates and Thermal Isomerization

Decay of Lumi II produces a second equilibrated mixture, USI 4, with similarities to the Meta I ⇄ Meta II equilibrium of rhodopsin. Given the time scale of its formation, presumably this mixture represents the first appearance of the G-protein activating species. The evolution of this mixture into USI 5 may have more parallels with Meta III formation in

the rhodopsin system which has been shown to involve anti-syn isomerization of the SB linkage (31). It would not be surprising that cone pigment Meta III formation should be faster than is seen in rod pigments, since cones require a faster response time. It is somewhat surprising that a PSB chromophore forms in these UV pigments, but this can be rationalized as being required for SB hydrolysis and ultimately enzymatic regeneration (32). Alternatively, in another cone pigment it has been proposed that a thermal regeneration pathway exists (33,34), while in bacteriorhodopsin a red shift has been proposed to be obligatory for thermal isomerization of the retinal (35,36). This may be involved in the case of these UV cone late photointermediates as well.

Given the prevalence and functional importance of protonated Schiff base chromophores in most visual pigments, it is remarkable that UV cone pigments with unprotonated SBs exist at all. Indeed, eliminating the pigment PSB in SHUV removes one of the earliest "locks" on the dark state found in all other classes of retinal based visual pigments. However, our observation here of SB protonation in SHUV's late fourth and fifth photointermediates may be another, possibly related, SB protonation anomaly of this UV cone pigment. Since the dark-state SHUV is converted to a Meta II-like unprotonated photointermediate upon photobleaching with 365-nm light, as observed using UV-visible spectroscopy (5), our observations of photointermediates with protontated SB in various time scales using transient absorption spectroscopy suggest that the photoactivation of SHUV involves multiple changes of the SB protonation state.

Abbreviations

Batho	bathorhodopsin
BSI	blue-shifted intermediate
DM	n-dodecyl-β-D-maltoside
GPCR	G protein-coupled receptor
Lumi	lumirhodopsin
Meta	metarhodopsin
MUV	mouse ultraviolet cone visual pigment
PSB	protonated N-retinylidene Schiff base
SB	N-retinylidene Schiff base
SHUV	Siberian hamster ultraviolet cone visual pigment
USI	unidirectional sequential intermediate
USID	unidirectional sequential intermediate difference
VCOP	*Xenopus laevis* violet cone pigment

REFERENCES

1. Bowmaker JK. Evolution of vertebrate visual pigments. Vision Res. 2008; 48:2022–2041. [PubMed: 18590925]
2. Yokoyama S. Evolution of dim-light and color vision pigments. Annu. Rev. Genom. Human Genet. 2008; 9:259–282.
3. Shichida Y, Matsuyama T. Evolution of opsins and phototransduction. Philos. T. Roy. Soc. B. 2009; 364:2881–2895.
4. Hunt DM, Carvalho LS, Cowing JA, Davies WL. Evolution and spectral tuning of visual pigments in birds and mammals. Philos. T. Roy. Soc. B. 2009; 364:2941–2955.

5. Mooney VL, Rivalta I, Neitz M, Neitz J, Sakmar TP, Kazmi MA, Lewis JW, Szundi I, Kliger DS, Batista VS, Yan ECY. Evidence that Schiff Base Protonation in Ultraviolet Cone Pigments is Regulated by Active Site Polar Residues, Water Molecules, and H-bonds. submitted.
6. Babu KR, Dukkipati A, Birge RR, Knox BE. Regulation of phototransduction in short-wavelength cone visual pigments via the retinylidene Schiff base counterion. Biochemistry. 2001; 40:13760–13766. [PubMed: 11705364]
7. Williams GA, Jacobs GHJ. Absence of functional short-wavelength sensitive cone pigments in hamsters (Mesocricetus). Comp. Physiol. A Neuroethol. Sens. Neural Behav. Physiol. 2008; 194:429–439.
8. Reeves PJ, Kim JM, Khorana HG. Structure and function in rhodopsin: A tetracycline-inducible system in stable mammalian cell lines for high-level expression of opsin mutants. Proc. Natl. Acad. Sci. U.S.A. 2002; 99:13413–13418. [PubMed: 12370422]
9. Oprian DD, Molday RS, Kaufman RJ, Khorana HG. Expression of a synthetic bovine rhodopsin gene in monkey kidney-cells. Proc. Natl. Acad. Sci. U.S.A. 1987; 84:8874–8878. [PubMed: 2962193]
10. Franke RR, Sakmar TP, Graham RM, Khorana HG. Structure and function in rhodopsin - Studies of the interaction between the rhodopsin cytoplasmic domain and transducin. J. Biol. Chem. 1992; 267:14767–14774. [PubMed: 1634520]
11. Epps J, Lewis JW, Szundi I, Kliger DS. Lumi I → Lumi II: The last detergent independent process in rhodopsin photoexcitation. Photochem. Photobiol. 2006; 82:1436–1441. [PubMed: 16553464]
12. Hug SJ, Lewis JW, Einterz CM, Thorgeirsson TE, Kliger DS. Nanosecond photolysis of rhodopsin: Evidence for a new blue-shifted intermediate? Biochemistry. 1990; 29:1475–1485. [PubMed: 2334708]
13. Szundi I, Lewis JW, Kliger DS. Deriving reaction mechanisms from kinetic spectroscopy. Application to late rhodopsin intermediates. Biophys. J. 1997; 73:688–702. [PubMed: 9251787]
14. Yoshzawa T, Wald G. Pre-lumirhodopsin and bleaching of visual pigments. Nature (Lond.). 1963; 197:1279. [PubMed: 14002749]
15. Shichida Y, Okada T, Kandori H, Fukada Y, Yoshizawa T. Nanosecond laser photolysis of iodopsin, a chicken red-sensitive cone visual pigment. Biochemistry. 1993; 32:10832–10838. [PubMed: 8399233]
16. Lewis JW, Liang J, Ebrey TG, Sheves M, Livnah N, Kuwata O, Jäger S, Kliger DS. Early photolysis intermediates of gecko and bovine artificial visual pigments. Biochemistry. 1997; 36:14593–14600. [PubMed: 9398178]
17. Dartnall, HJA. The Photobiology of Visual Processes. In: Davson, H., editor. The Eye. Vol. vol. 2. New York: Academic Press; 1962. p. 323-533.
18. Lewis JW, Szundi I, Fu WY, Sakmar TP, Kliger DS. pH dependence of photolysis intermediates in the photoactivation of rhodopsin mutant E113Q. Biochemistry. 2000; 39:599–606. [PubMed: 10642185]
19. Sakmar TP, Franke RR, Khorana HG. The role of the retinylidene Schiff-base counterion in rhodopsin in determining wavelength absorbency and Schiff-base pK_a. Proc. Natl. Acad. Sci. U.S.A. 1991; 88:3079–3083. [PubMed: 2014228]
20. Shi YS, Radlwimmer FB, Yokoyama S. Molecular genetics and the evolution of ultravioletvision in vertebrates. Proc. Natl. Acad. Sci (USA). 2001; 98:11731–11736. [PubMed: 11573008]
21. Hunt DM, Carvalho LS, Cowing JA, Parry JWL, Wilkie SE, Davies WL, Bowmaker JK. Spectral Tuning of Shortwave-sensitive Visual Pigments in Vertebrates. Photochem. Photobiol. 2007; 83:303–331. [PubMed: 17576346]
22. Palings I, van den Berg EMM, Lugtenburg J, Mathies RA. Complete assignment of the hydrogen out-of-plane wagging vibrations of bathorhodopsin - Chromophore structure and energy-storage in the primary photoproduct of vision. Biochemistry. 1989; 28:1498–1507. [PubMed: 2719913]
23. Lin SW, Groesbeek M, van der Hoef I, Verdegem P, Lugtenburg J, Mathies RA. Vibrational Assignment of Torsional Normal Modes of Rhodopsin: Probing Excited-State Isomerization Dynamics along the Reactive C_{11}=C_{12} Torsion Coordinate. J. Phys. Chem. B. 1998; 102:2787–2806.

24. Yan ECY, Epps J, Lewis JW, Szundi I, Bhagat A, Sakmar TP, Kliger DS. Photointermediates of the rhodopsin S186A mutant as a probe of the hydrogen-bond network in the chromophore pocket and the mechanism of counterion switch. J. Phys. Chem. C. 2007; 111:8843–8848.
25. Nakamichi H, Okada T. Crystallographic Analysis of Primary Visual Photochemistry. Angew. Chem. Int. Ed. 2006; 45:4270–4273.
26. Kliger DS, Lewis JW. Spectral and kinetic characterization of visual pigment photointermediates. Isr. J. Chem. 1995; 35:289–307.
27. Pan D, Ganim Z, Kim JE, Verhoeven MA, Lugtenburg J, Mathies RA. Time-resolved resonance Raman analysis of chromophore structural changes in the formation and decay of rhodopsin's BSI intermediate. J. Am. Chem. Soc. 2002; 124:4857–4864. [PubMed: 11971736]
28. Ramos LS, Chen Min-H, Knox BE, Birge RR. Regulation of Photoactivation in Vertebrate Short Wavelength Visual Pigments: Protonation of the Retinylidene Schiff Base and a Counterion Switch. Biochemistry. 2007; 46:5330–5340. [PubMed: 17439245]
29. Szundi I, Epps J, Lewis JW, Kliger DS. Temperature Dependence of the Lumirhodopsin I-Lumirhodopsin II Equilibrium. Biochemistry. 2010; 49:5852–5858. [PubMed: 20545328]
30. Dukkipati A, Kusnetzow A, Babu KR, Ramos L, Singh D, Knox BE, Birge RR. Phototransduction by Vertebrate Ultraviolet Visual Pigments: Protonation of the Retinylidene Schiff Base following Photobleaching. Biochemistry. 2002; 41:9842–9851. [PubMed: 12146950]
31. Vogel R, Siebert F, Mathias G, Tavan P, Fan G, Sheves M. Deactivation of Rhodopsin in the Transition from the Signaling State Meta II to Meta III Involves a Thermal Isomerization of the Retinal Chromophore C=N Double Bond. Biochemistry. 2003; 42:9863–9874. [PubMed: 12924935]
32. Heck M, Schädel SA, Maretzki D, Bartl FJ, Ritter E, Palczewski K, Hofmann KP. Signaling States of Rhodopsin Formation of the storage form, metarhodopsin III, from active metarhodopsin II. J. Biol. Chem. 2003; 278:3162–3169. [PubMed: 12427735]
33. Imamoto Y, Imai H, Yoshizawa T, Shichida Y. Thermal recovery of iodopsin from its meta I-intermediate. FEBS Letters. 1994; 354:165–168. [PubMed: 7957918]
34. Imamoto Y, Shichida Y. Thermal Recovery of Iodopsin from Photobleaching Intermediates. Photochem. Photobiol. 2008; 84:941–948. [PubMed: 18399920]
35. Milder SJ. Correlation between absorption maxima and thermal isomerization rates in bacteriorhodopsin. Biophys. J. 1991; 60:440–446. [PubMed: 19431800]
36. Balashov SP, lmasheva ES, Govindjee R, Ebrey TG. Titration of Aspartate-85 in Bacteriorhodopsin: What It Says About Chromophore Isomerization and Proton Release. Biophys. J. 1996; 70:473–481. [PubMed: 8770224]

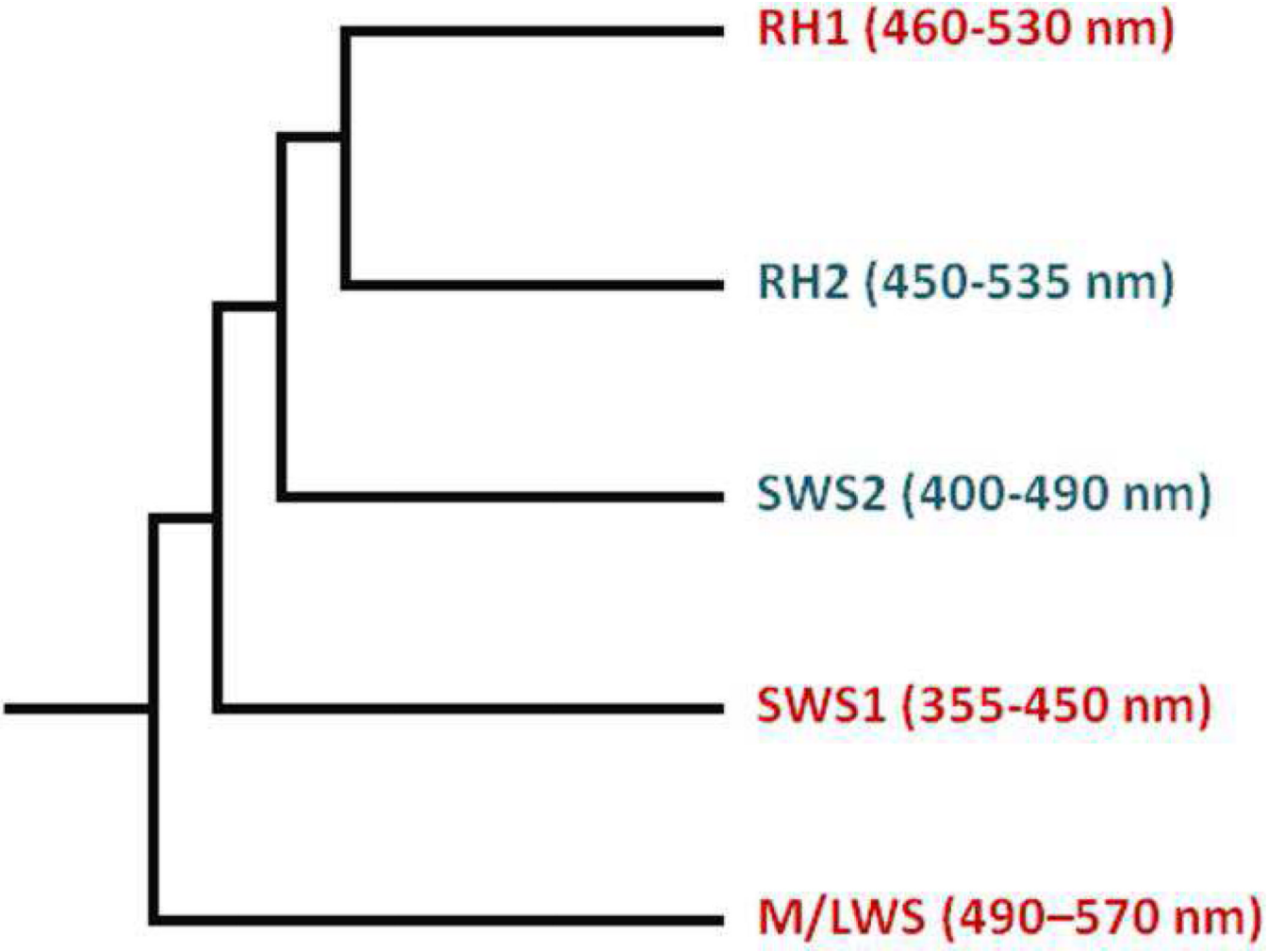

Figure 1. Evolutionary cladogram of the five classes of vertebrate visual pigments
RH2 and SWS2 are no longer expressed in mammals. (1–4)

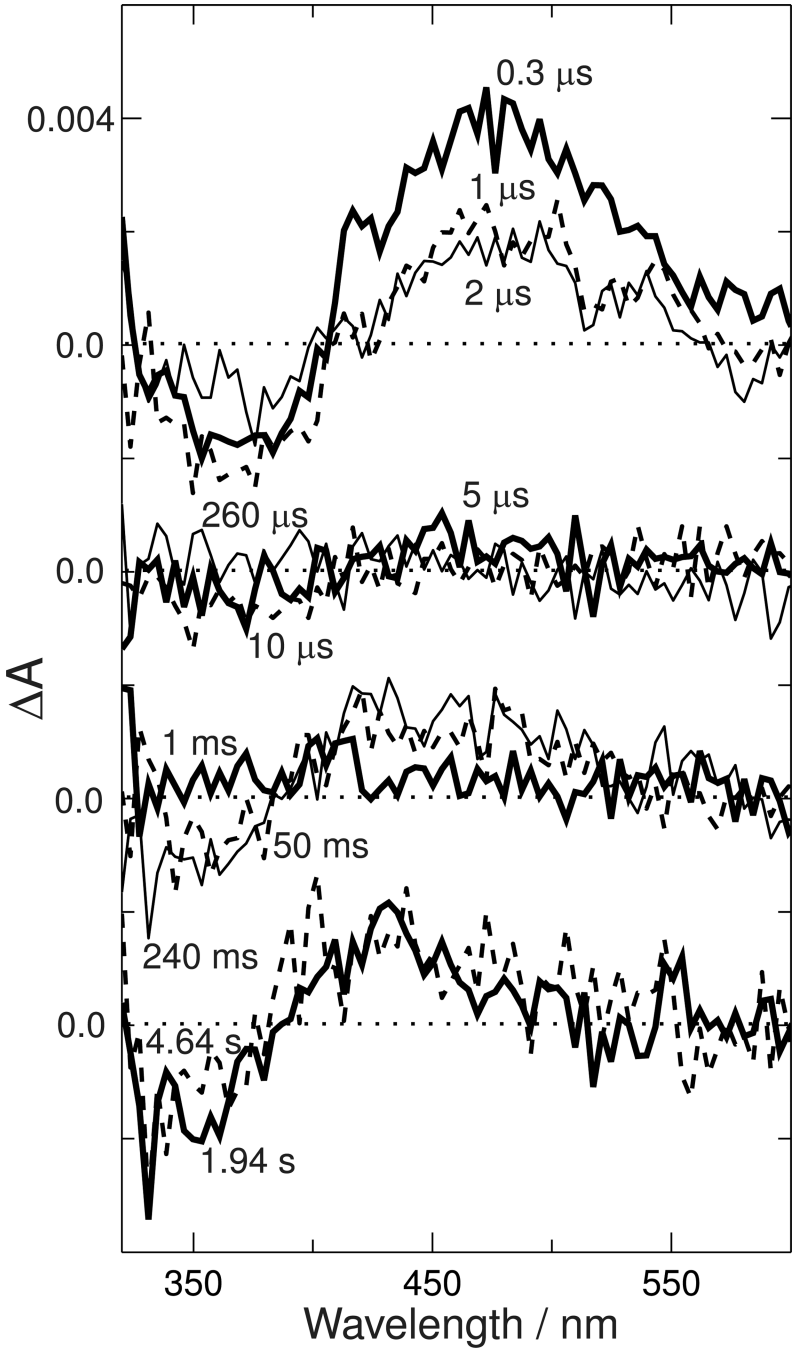

Figure 2. Absorbance changes after photoexcitation of Siberian hamster ultraviolet cone pigment

Absorbance difference spectra were collected at the indicated delays after 355 nm photoexcitation, with each successive set of curves offset downward by 0.004 absorbance units for clarity. Approximately 120 μg of pigment was consumed in this series of measurements, and each trace is the average of approximately 40 individual photoexcitation pulses conducted on fresh 1 μL aliquots of pigment solution. Delay times are as follows: top panel 0.3 μs (heavy line), 1 μs (dashed line) and 2 μs (light line); second panel 5 μs (heavy line), 10 μs (dashed line) and 260 μs (light line); third panel 1 ms (heavy line), 50 ms (dashed line) and 240 ms (thin line); bottom panel 1.94 sec (heavy line) and 4.64 sec (dashed line).

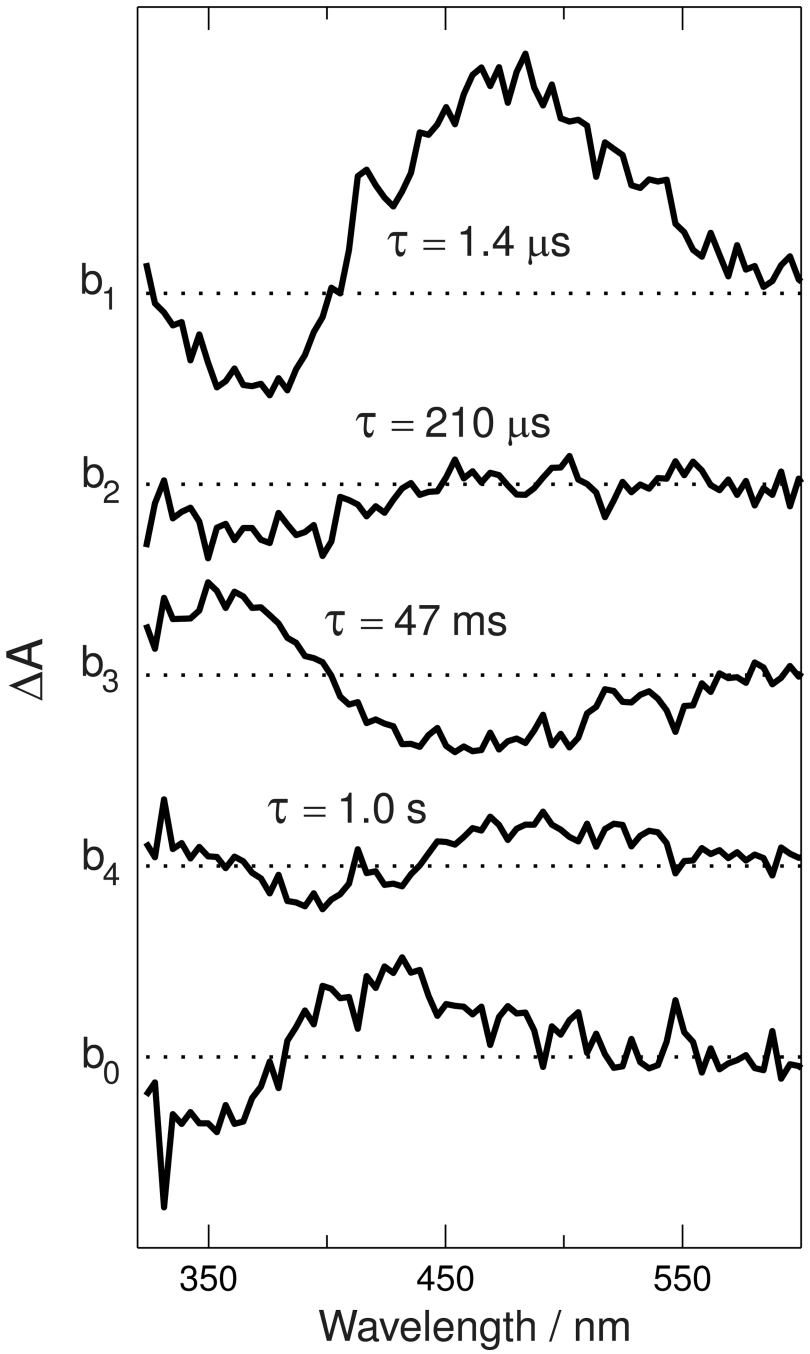

Figure 3. Spectral coefficients (b-spectra) of time decaying exponentials fit to Siberian hamster UV cone pigment data

The data in Figure 2 were fit to a function containing four exponential terms (with lifetimes indicated), whose coefficient b-spectra, $b_1(\lambda)...b_4(\lambda)$, are plotted above, and a time-independent term, $b_0(\lambda)$, which is plotted at the bottom. Spacing between the curves is 0.004 absorbance units.

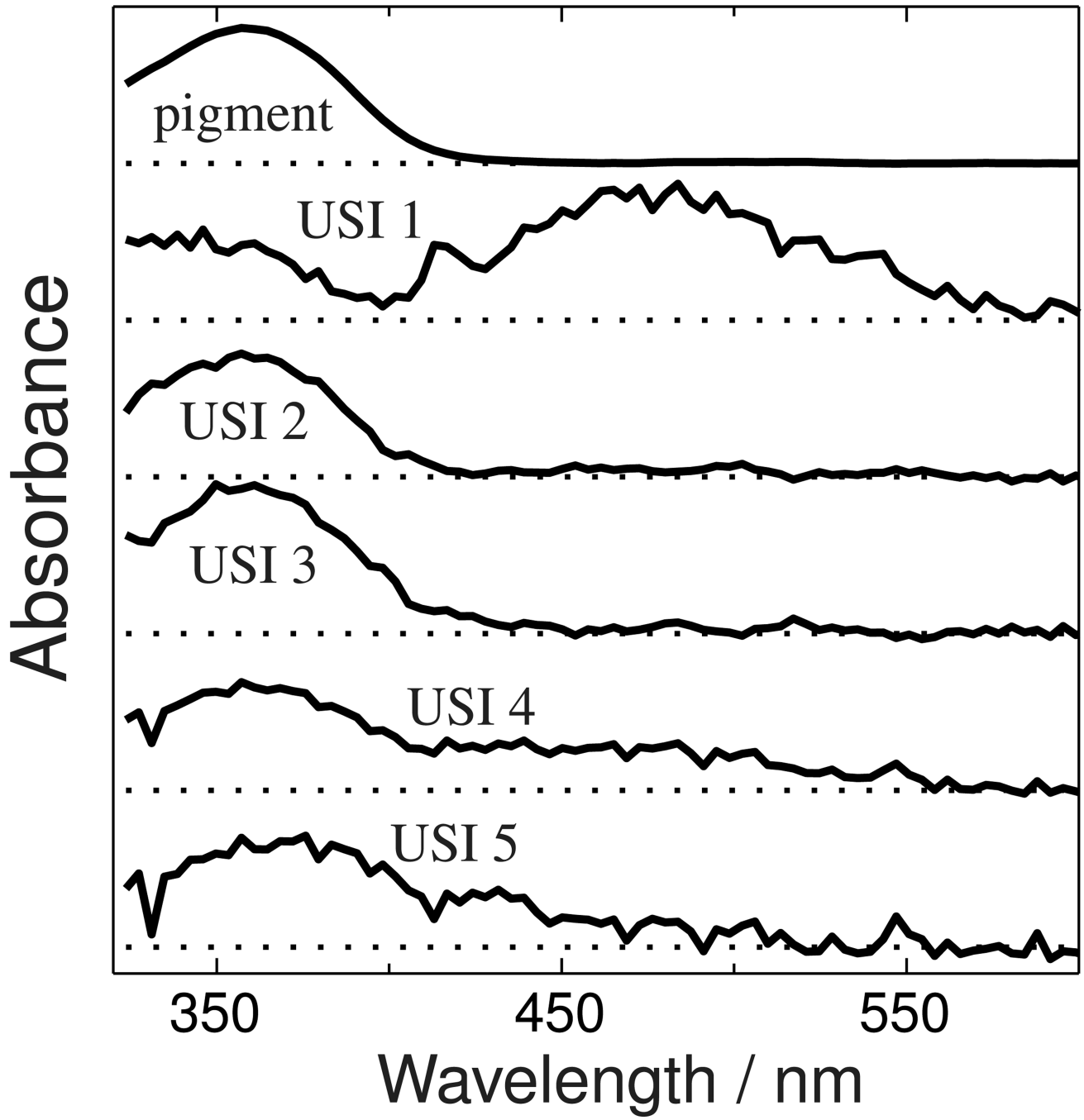

Figure 4. Unidirectional sequential intermediate (USI) spectra

The absorbance spectrum of the Siberian hamster UV pigment is plotted at the top, and under it are the absolute spectra of the five species that appear after its photoexcitation. The USI spectra are hypothetical photointermediate spectra calculated under the assumption that a unidirectional sequential scheme is followed. USI spectra that are more complex than the original pigment spectrum (e.g. 1, 4 and 5) suggest that those USI species are mixtures of two photointermediates which equilibrate on a time scale faster than that associated with the USI's formation.

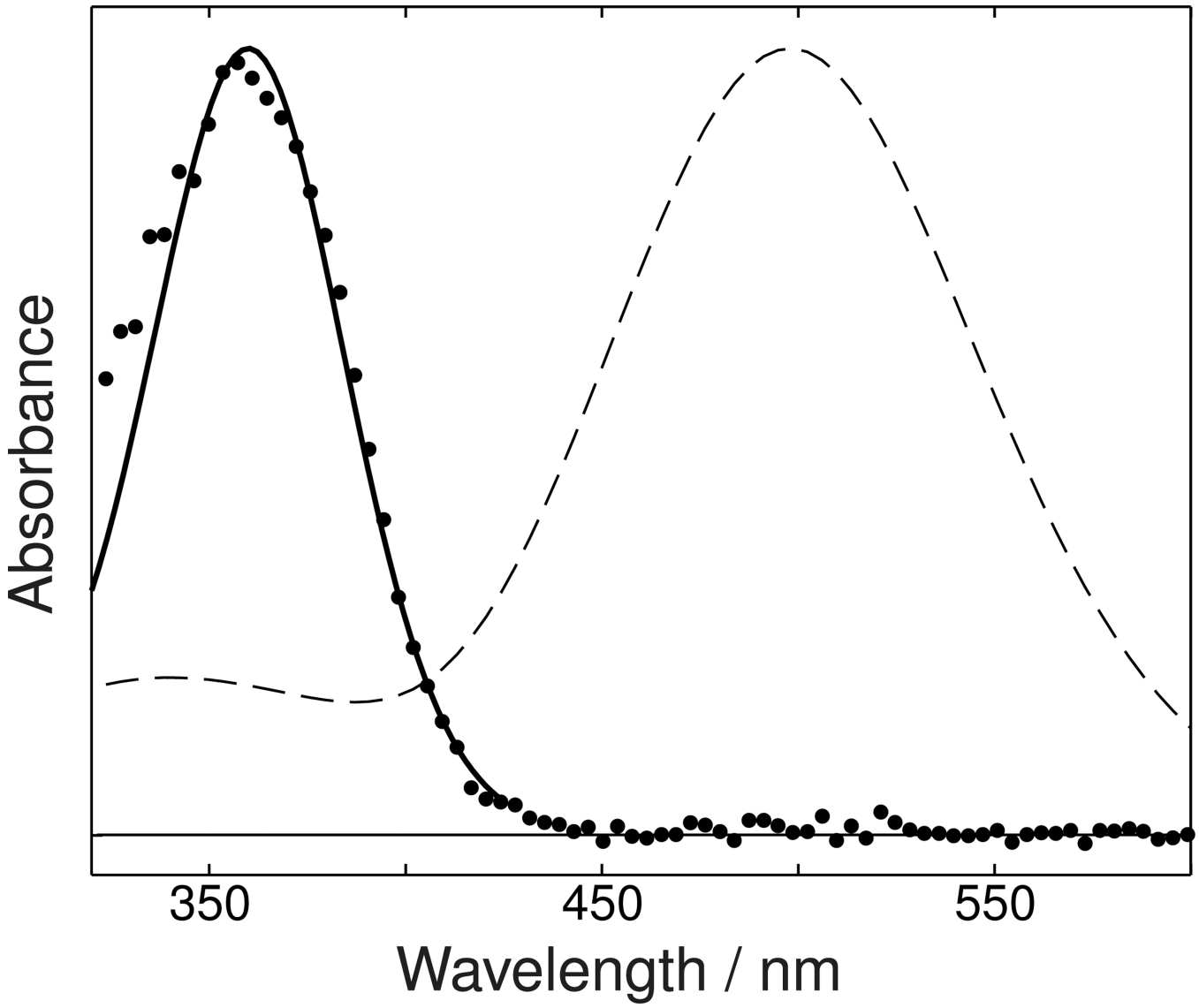

Figure 5. Siberian hamster UV pigment absorbance compared to energy shifted bovine rhodopsin spectrum

Points show the absorbance of a DM suspension of Siberian hamster UV cone pigment. The absorbance of bovine rhodopsin in a detergent suspension is shown by the dashed line. The solid line shows the result of shifting the bovine rhodopsin spectrum to the same wavelength of maximum absorbance as the Siberian hamster UV pigment with its width scaled to be the same in energy units as the 498 nm bovine rhodopsin absorbance band.

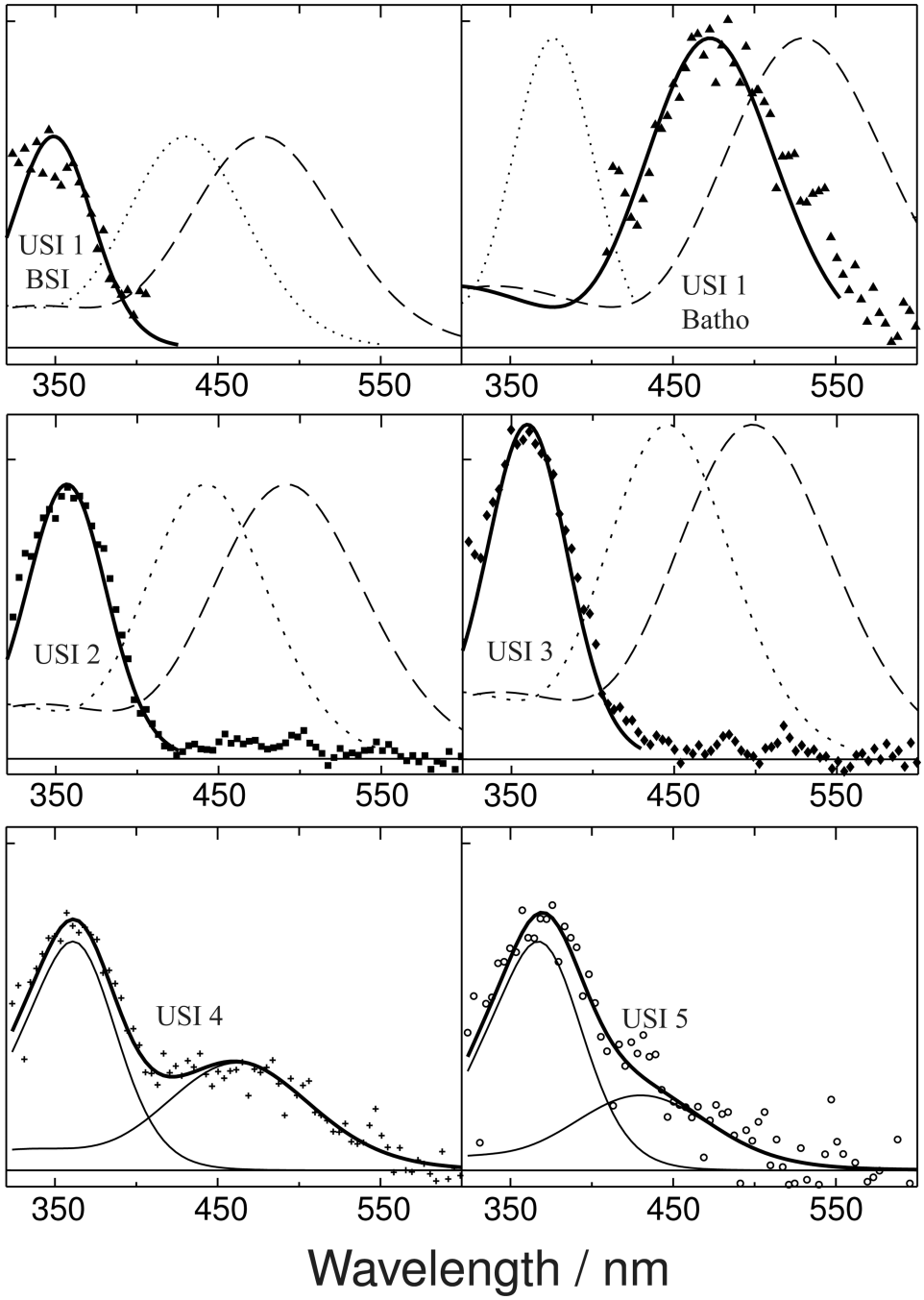

Figure 6. USI spectra fitted to model photointermediate components

The absorbance of USI 1, shown in Figure 4, has both UV and visible bands which suggests that USI 1 is an equilibrated mixture of two photointermediate species whose equilibration is fast. The top left panel above shows how the UV portion of USI 1's absorbance (▲) can be modeled in terms of a deprotonated SB form (solid line, see text for model details) analogous to bovine rhodopsin's BSI intermediate (dashed line). The dotted line in the same panel, which does not fit the UV portion of the USI 1 data, shows the corresponding PSB form of the model BSI for Siberian hamster UV cone pigment. The top right panel shows how the visible absorbing portion of USI 1's absorbance models well as a PSB form (solid line) analogous to bovine rhodopsin's Batho intermediate (dashed line), but not as a

deprotonated SB form of Siberian hamster Batho (dotted line). Similarly, the middle panels show how absorbance of both USI 2 (■) and USI 3 (♦) are well fit by deprotonated SB forms of the model Siberian hamster Lumi I and Lumi II spectra (solid lines), derived from the bovine Lumi I and Lumi II (dashed lines) but not by model PSB forms of those photointermediates (dotted lines). The lower panels show how absorbance of USIs 4 (+) and 5 (○) can be decomposed into two bands, presumably corresponding to mixtures of protonated and deprotonated SB species, but the correspondence of these components to bovine rhodopsin photointermediates is not clear.

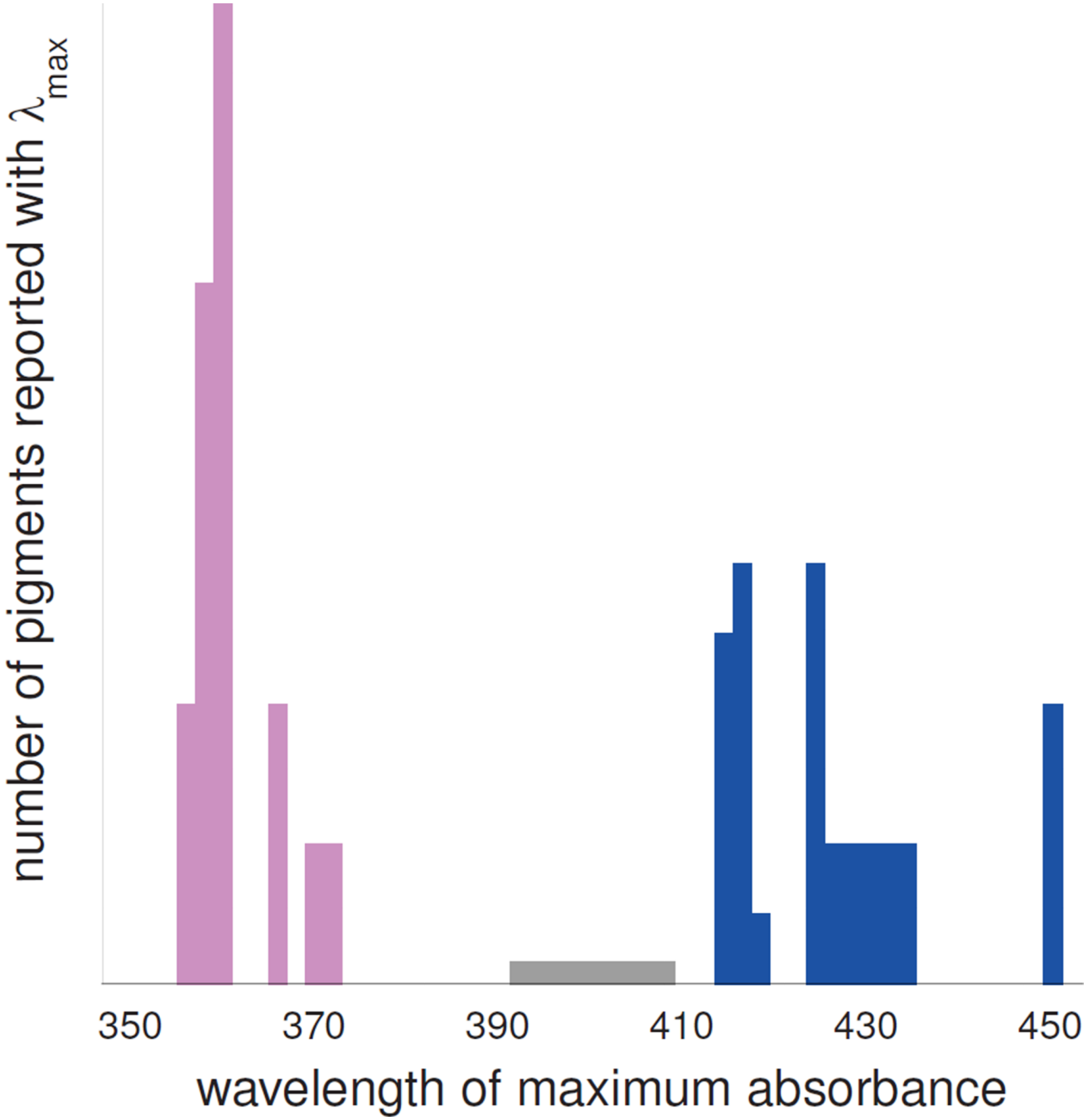

Figure 7. Histogram of reported UV cone and violet cone cone pigment λ_{max} values

Blue bars on right represent violet cone pigments from human, macaque monkey, marmoset, squirrel monkey, cow, chicken and frog. Magenta bars on the left represent UV cone pigments from house mouse, rat, golden hamster, parakeet, canary, zebra finch, tiger salamander, chameleon and goldfish. The gray bar from 393 to 409 nm represents the violet cone pigment from domestic pigeon which has been reported to have variable λ_{max} in this range. Similarly, for the other pigments where a range of λ_{max} values were reported, bars of reduced height occur at the corresponding wavelengths.